Supplementary Information

Quasi-2D MIL-100 (Fe) Synthesis via Benzene-1,3,5-Tricarboxylic Acid Self-Assembly: Organic Dye Adsorption at Room Temperature with Dramatically Enhanced Kinetics

Ghazal Rabiee[1], Alireza Abbasi[1], Mohammad Behbahani[2]*

[1]School of Chemistry, College of Science, University of Tehran, Tehran, Iran

[2]Department of Chemistry, Faculty of Science, Shahid Chamran University of Ahvaz, Ahvaz, Iran

**E-mail: a_abbasi@ut.ac.ir*

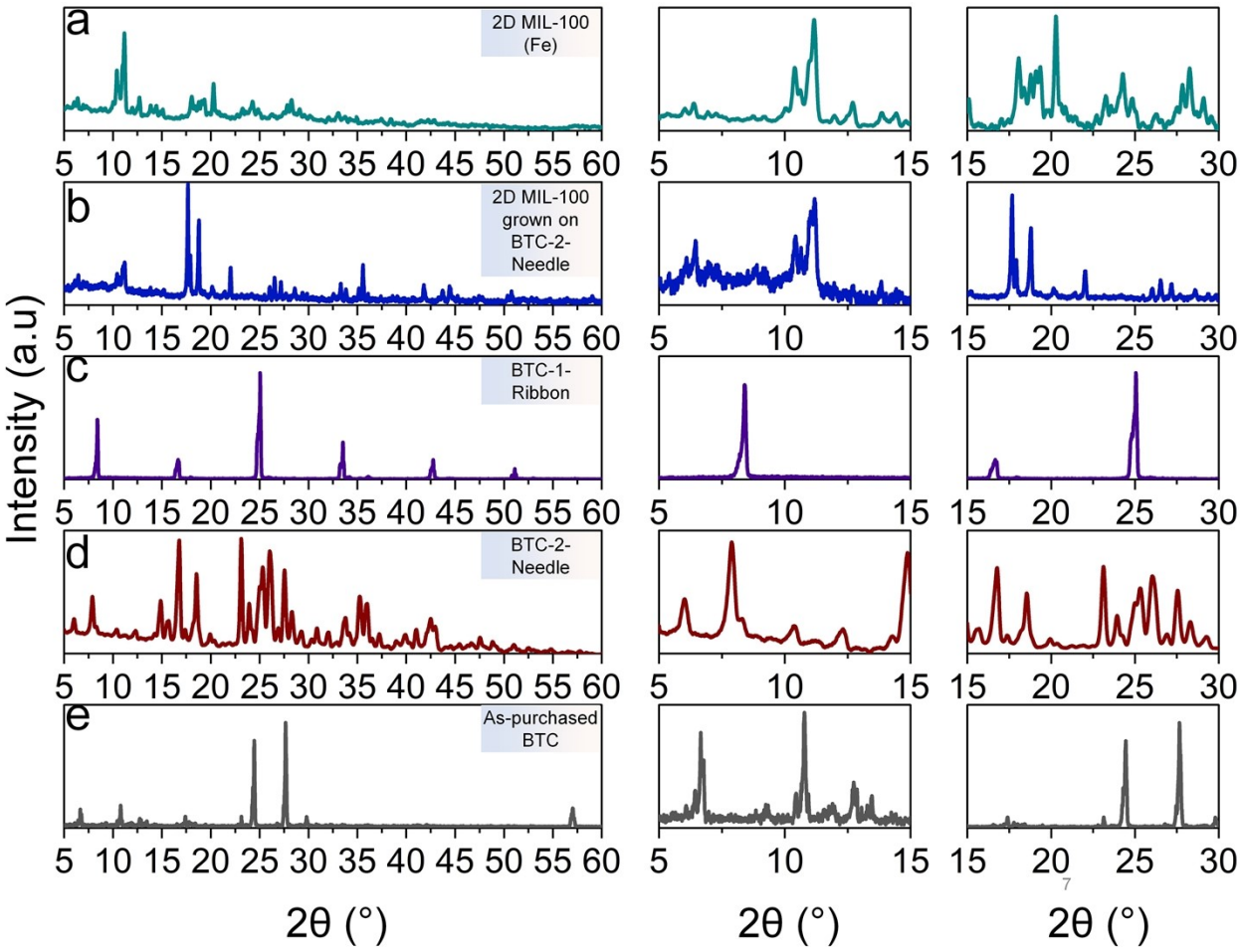

Fig. S1. *X-ray diffraction analysis. (a) Patterns collected for quasi-2D MIL-100 (Fe) sample synthesized under optimized conditions and (b) patterns collected for needle-like structures presented in Fig. 1 in the main manuscript (grown on* ***BTC-2-Needle****). Here, the green labels show the matching diffractions between the two samples, and the red labels show extra unidentified diffraction, suggesting the formation of both the quasi-2D MIL-100 (Fe) phase and other secondary phases based on the interaction of BTC and Fe sources. Patterns collected for recrystallized BTC as (c) BTC-1-Ribbon, (d) BTC-2-Needle, and (e) as purchased BTC. The magnified portions of interest in each plot are shown on the right panels.*

Fig. S1 displays the XRD patterns for the quasi-2D MIL-100 (Fe), Needle-like structures shown in Fig. 2, and XRD patterns of benzene-1,3,5-tricarboxylic acid (BTC) prepared through various crystallization processes. The principal objective of this analysis was to determine the source of contaminants in the needle-like structures and to investigate various assemblies of BTC molecules. XRD pattern for samples prepared under optimized conditions from BTC-1-Ribbon (Fig. S1 (a)) exhibits dominant peaks associated with MIL-100 (Fe) with no significantly detectable impurity peaks, consistent with the data in existing literature [1-3]. Fig. S1 (b) shows the XRD peaks of MIL-100 (Fe) particles (2Θ=5-15) as well as noticeably sharp and unidentified peaks within 2Θ=15°-30° and at the higher end of the 2θ scale. These peaks do not originate from starting materials and might stem from needle-like structures shown in Fig. 2 (main text). It is noteworthy to mention that the needle-like structures are not pure BTC-1-Needle anymore and have incorporated iron species in their structure and we do not expect to see the original BTC-1-Needle peaks in this sample. Fig. S1 (c) shows the XRD pattern for the self-assembled BTC molecules with a great degree of texture [4]. This texture, resulting from the highly aligned orientation of crystals within the polycrystalline sample, manifests in our XRD data as an unusually high signal-to-noise (S/N) ratio, which corroborates the formation of highly oriented ribbons. Fig. S1 (d and e) display the XRD pattern for the recrystallized BTC molecules in the form of needles (BTC-2-Needle) and the as-purchased BTC ligand.

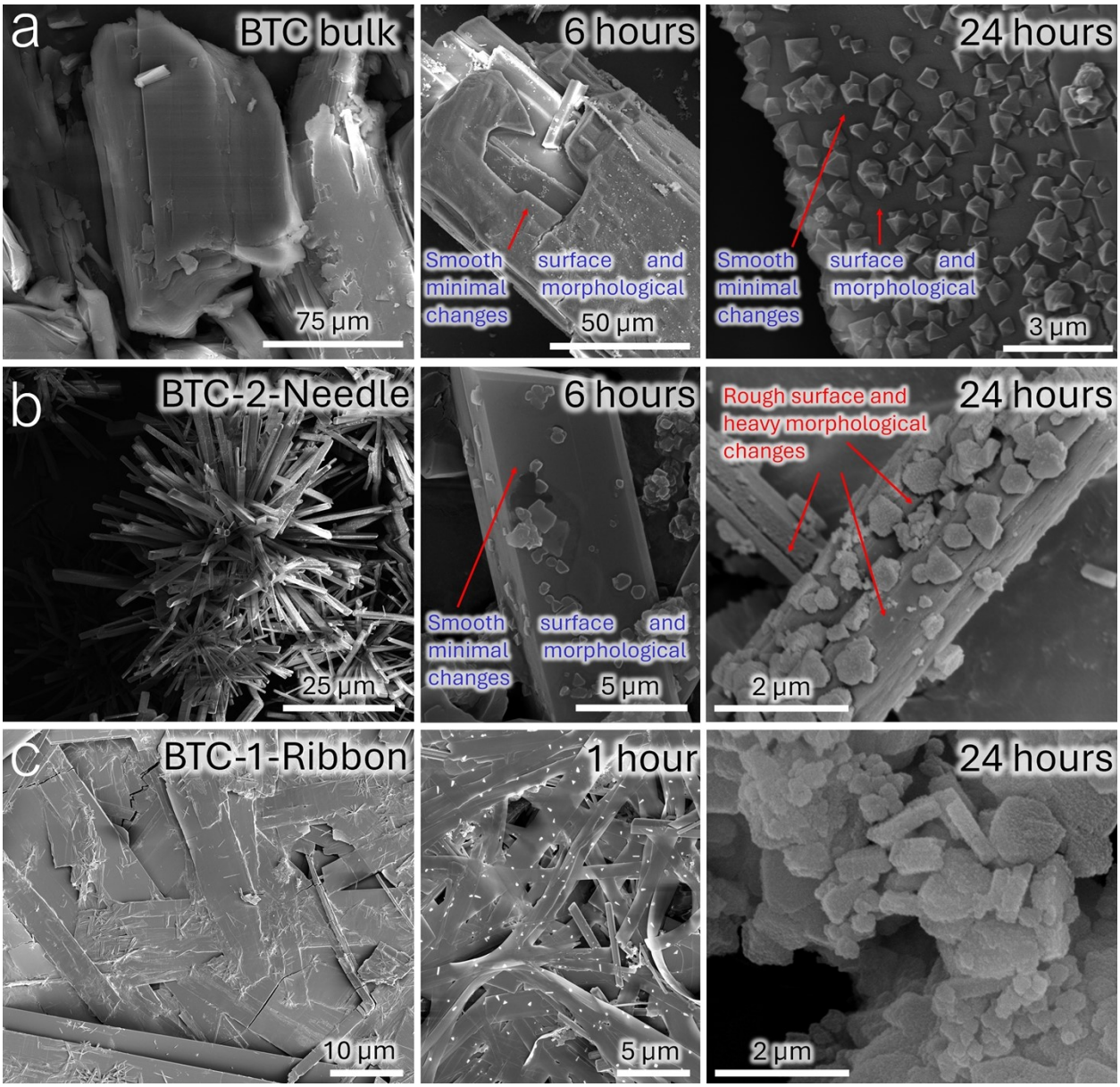

Fig. S2. *Scanning electron microscopy analysis. (a) Bulk BTC before the synthesis, 6 and 24 hours into the synthesis. (b) BTC-2-Needle BTC before the synthesis, 6 and 24 hours into the synthesis. (c)BTC-1-Ribbon BTC before the synthesis, 1 and 24 hours into the synthesis.*

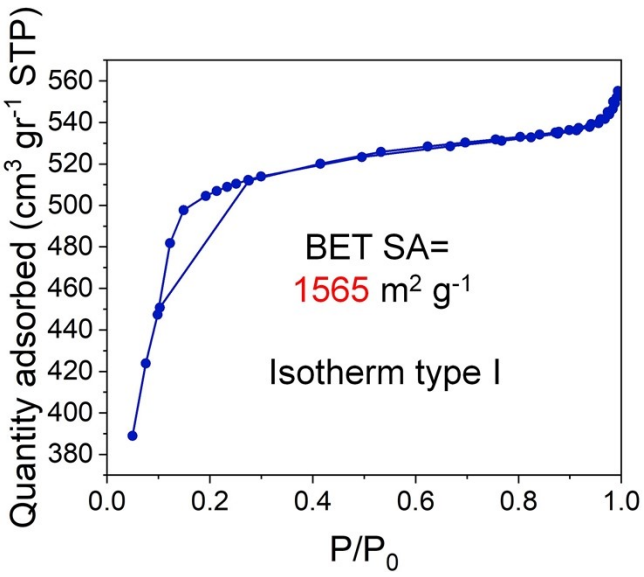

Fig. S3. *The BET analysis of 3D MIL-100 (Fe) made via traditional synthesis route.*

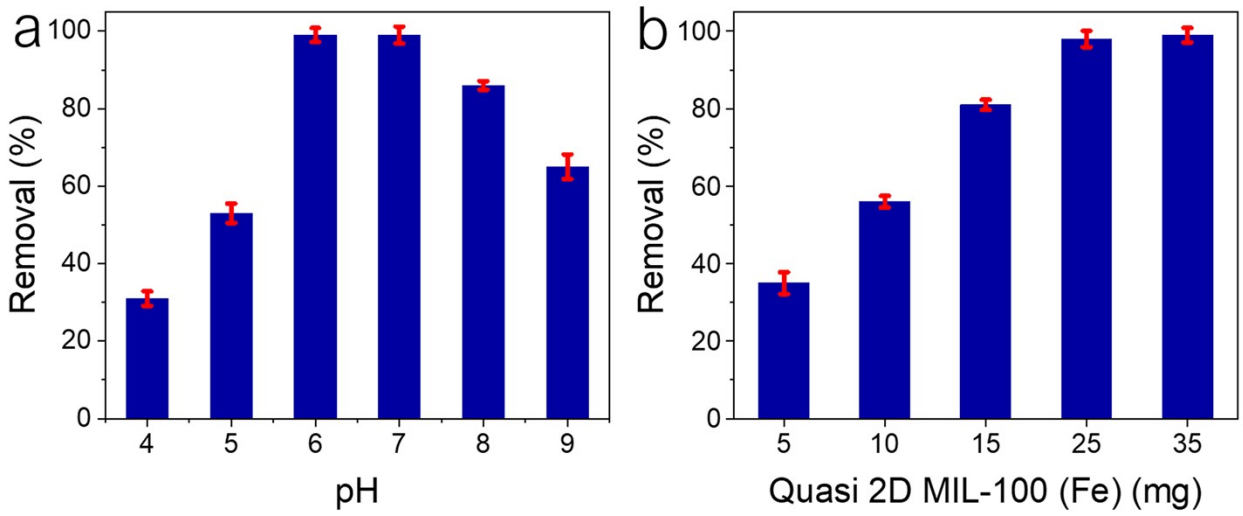

Fig. S4. *The effect of (a) pH and (b) adsorbent mass on adsorption of RhB via quasi-2D MIL-100 (Fe).*

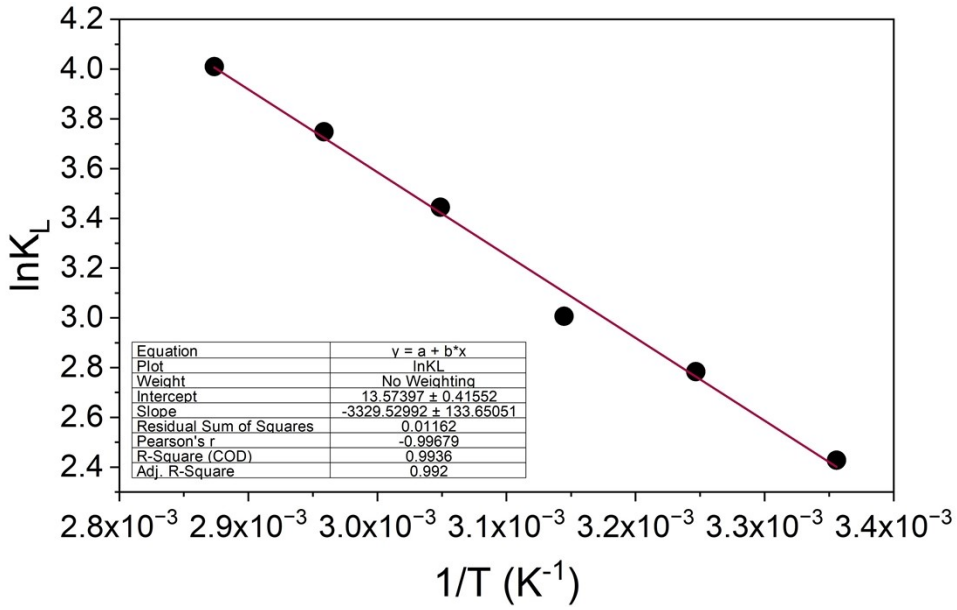

Fig. S5. *Van't Hoff plot for the adsorption of RhB via quasi-2D MIL-100 (Fe).*

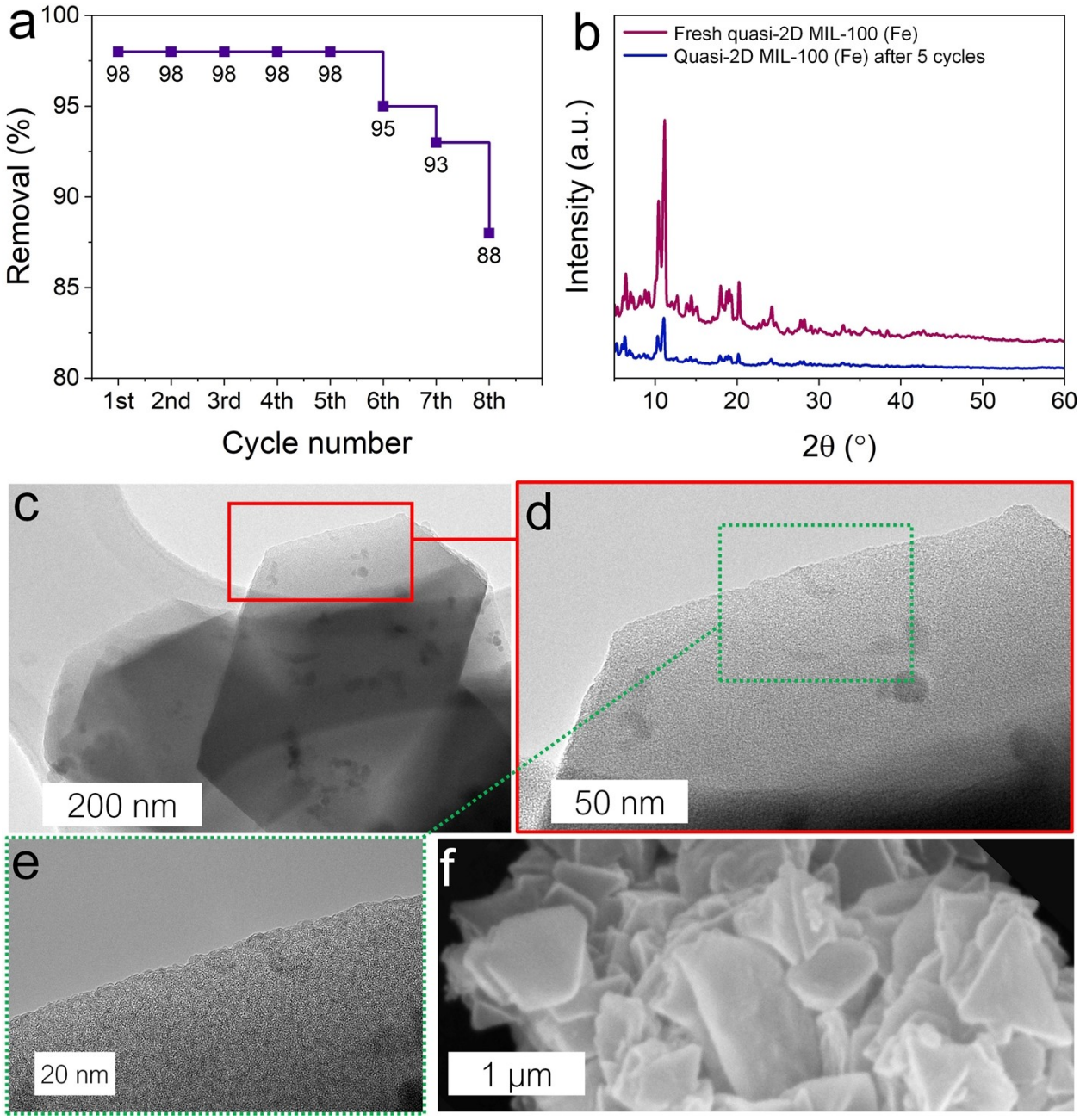

Fig. S6. *Performance assessment and structural analysis of used adsorbent. (a) Reusability of the quasi-2D MIL-100 (Fe) up to 8 cycles. (b) the XRD pattern of the used quasi-2D MIL-100 (Fe) after multiple time reuse compared to the fresh adsorbent. (c-e) TEM micrograph of the used sample showing the Q2D structure and higher resolution images showing no significant signs of degradation, and (f) an SEM image of the use quasi-2D MIL-100 (Fe) with a Q2D morphology.*

Table S1. Adsorption kinetic and isotherm data.

Kinetic parameters					
Pseudo-first Model			**Pseudo-second Model**		
Q_e (mg g^{-1})	R^2	K_1 (min^{-1})	Q_e (mg g^{-1})	R^2	K_2 (g mg^{-1} min^{-1})
27.8	0.869	0.05	30.3	0.991	0.00364
Isotherm parameters					
Langmuir Model			**Freundlich Model**		
Q_m (mg g^{-1})	R^2	B (L mg^{-1})	K_f	R^2	n
86.5	0.994	1.7	4.85	0.952	4.2

Table S2. Removal of RhB organic dye by metal-organic frameworks

Adsorbent	Mass (mg)	Time (min)	pH	T (ºC)	Isotherm model	Adsorption capacity (Q, mg g^{-1})	Kinetics model	Ref.
Fe_3O_4/Conventional MIL-100(Fe)	20	120	4-8	RT	Freundlich	28	Pseudo-second order	[5]
Conventional MIL-100 (Fe)	100	360	4-10	RT	Langmuir	61.9	Elovich	[6]
Nanoscale MIL-100 (Fe)	30	Up to 30	6	RT	Langmuir	76	Pseudo-second order	[7]
Conventional MIL-100 (Fe)	25	400	6	RT	Langmuir	62	Pseudo-second order	This work
Quasi-2D MIL-100 (Fe)	25	90	6	RT	Langmuir	86.5	Pseudo-second order	This work

References

1. W. J. He, H. P. Jia, Z. P. Li, C. Q. Miao, R. H. Lu, S. B. Zhang and Z. Q. Zhang, *Journal of Environmental Chemical Engineering*, 2022, **10**, 108698.
2. T. T. He, W. Liu, T. Lev, M. S. Ma, Z. F. Liu, A. Vasiliev and X. G. Li, *Sensors and Actuators B: Chemical* 2021, **329**, 129275.
3. P. Horadada, S. Surble, C. Serre, D. Y. Hong, Y. K. Seo, J. S. Chang, J. M. Greneche, I. Margiolaki and G. Ferey, *Chem Commun (Camb)*, 2007, DOI: 10.1039/b704325b, 2820-2822.
4. C. F. Holder and R. E. Schaak, *ACS Nano*, 2019, **13**, 7359-7365.
5. H. Liu, X. Ren and L. Chen, *Journal of Industrial and Engineering Chemistry*, 2016, **34**, 278-285.
6. H. Y. Jang, J. K. Kang, J. A. Park, S. C. Lee and S. B. Kim, *Environ Pollut*, 2020, **267**, 115583.
7. S. Duan, J. Li, X. Liu, Y. Wang, S. Zeng, D. Shao and T. Hayat, *ACS Sustainable Chemistry & Engineering*, 2016, **4**, 3368–3378.